ACS OMEGA

http://pubs.acs.org/journal/acsodf

Article

Experimental Characterization of *In Silico* Red-Shift-Predicted iLOV$^{L470T/Q489K}$ and iLOV$^{V392K/F410V/A426S}$ Mutants

Pierre Wehler,[‖] Daniel Armbruster,[‖] Andreas Günter, Erik Schleicher, Barbara Di Ventura, and Mehmet Ali Öztürk*

Cite This: *ACS Omega* 2022, 7, 19555−19560

Read Online

ACCESS | Metrics & More | Article Recommendations | Supporting Information

ABSTRACT: iLOV is a flavin mononucleotide-binding fluorescent protein used for *in vivo* cellular imaging similar to the green fluorescent protein. To expand the range of applications of iLOV, spectrally tuned red-shifted variants are desirable to reduce phototoxicity and allow for better tissue penetration. In this report, we experimentally tested two iLOV mutants, iLOV$^{L470T/Q489K}$ and iLOV$^{V392K/F410V/A426S}$, which were previously computationally proposed by (Khrenova et al. *J. Phys. Chem. B* **2017**, *121* (43), pp 10018−10025) to have red-shifted excitation and emission spectra. While iLOV$^{L470T/Q489K}$ is about 20% brighter compared to the WT *in vitro*, it exhibits a blue shift in contrast to quantum mechanics/molecular mechanics (QM/MM) predictions. Additional optical characterization of an iLOV^{V392K} mutant revealed that V392 is essential for cofactor binding and, accordingly, variants with V392K mutation are unable to bind to FMN. iLOV$^{L470T/Q489K}$ and iLOV$^{V392K/F410V/A426S}$ are expressed at low levels and have no detectable fluorescence in living cells, preventing their utilization in imaging applications.

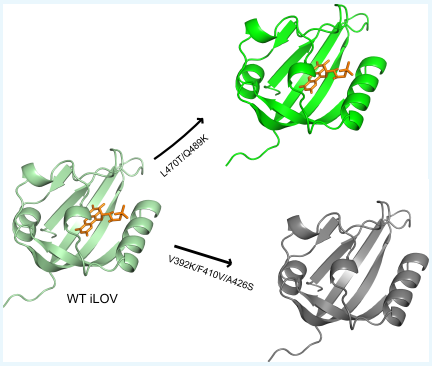

INTRODUCTION

Fluorescent proteins (FPs) have revolutionized cell biology by enabling researchers to investigate dynamic cellular processes in real time.[1] The most widely used FP is the green fluorescent protein (GFP) and its spectrally shifted and/or engineered variants,[1] which have been optimized, for instance, to mature more rapidly (sfGFP)[2] or fluoresce more brightly (mNeonGreen).[3] Despite their usefulness, FPs of the GFP family have some limitations: they depend on molecular oxygen for chromophore formation, which impedes their use to visualize processes under hypoxic or anoxic conditions,[4−6] are relatively large (∼25 kDa), which can be problematic in some applications,[7,8] and are mostly sensitive to pH.[9] While pH-resistant GFP variants have been engineered,[9] oxygen dependence and size are mostly unchangeable features. FMN-binding fluorescent proteins (FbFPs) can overcome these limitations and thus are valuable alternatives to GFP and its variants.[10,11] FbFPs consist of a small light oxygen voltage (LOV) domain (∼11 kDa) emitting green fluorescence when light in the UV-A-blue range reaches the noncovalently bound FMN chromophore.[12]

One prominent FbFP is iLOV, a derivative of the LOV2 domain of *Arabidopsis thaliana*.[7] A mutation in a key cysteine residue and several rounds of DNA shuffling led to enhanced fluorescence emission.[7] While FbFPs have been used in molecular imaging for more than a decade,[13] they suffer from the autofluorescence signal of flavin molecules in the cell and relatively weak fluorescent intensity, issues which have not been improved until very recently.[14,15] Engineering a red-shifted iLOV would bring several advantages, for instance, lower phototoxicity and deeper tissue penetration. Moreover, a red-shifted FbFP variant could be used orthogonally to other FbFPs and would potentially allow for multicolor imaging and FRET-based biosensors.

Based on the observation that the red fluorescent proteins Rtms5[16] and mKeima[17] possess positively charged residues in close proximity to the chromophore, Khrenova and colleagues applied quantum mechanics/molecular mechanics (QM/MM) simulations and proposed that the iLOV^{Q489K} mutant would have a ∼50 nm red shift in its excitation and emission maxima compared to wild-type (WT) iLOV.[18] Their rationale was that introducing a positively charged amino group at position 489 next to the chromophore would stabilize the π-electron system of the FMN in the excited singlet state. However, later Davari and colleagues computationally and experimentally showed that K489 is mostly populated in an open conformer and flipped away, which is far from the chromophore and in fact iLOV^{Q489K} is blue-shifted.[19] In a follow-up study, Khrenova and colleagues applied the second round of QM/MM

Received: March 3, 2022
Accepted: April 28, 2022
Published: June 1, 2022

https://doi.org/10.1021/acsomega.2c01283
ACS Omega 2022, 7, 19555−19560

calculations and found other mutations that were predicted to have more stabilized lysine residues next to the chromophore compared to iLOV^{Q489K}, which led them to propose iLOV$^{L470T/Q489K}$ and iLOV$^{V392K/F410V/A426S}$ as mutants with ~50 nm red shift for both excitation and emission spectra[20] (Figure 1). As a shift of such magnitude would open up new applications for iLOV and FbFPs in general, we experimentally tested these two mutants in this short report by measuring the absorption, excitation, and emission spectra and calculating the quantum yield and brightness of the purified proteins.

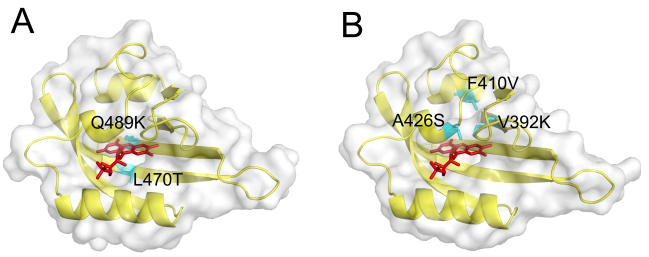

Figure 1. Model structures of iLOV$^{L470T/Q489K}$ and iLOV$^{V392K/F410V/A426S}$ mutants. Cartoon and surface representations of the iLOV$^{L470T/Q489K}$ (A) and iLOV$^{V392K/F410V/A426S}$ (B) mutants. Positions of mutations are shown in cyan. The structures (yellow) were generated using the Swiss-Model web-server[21] and the FMN (red) was placed by aligning the model structures to the WT iLOV X-ray structure (PDB id: 4EEP). Figures were generated using PyMOL.[22]

RESULTS

iLOV^{V392K}, iLOV$^{L470T/Q489K}$, and iLOV$^{V392K/F410V/A426S}$ are not Detectable in Living Cells. To experimentally test the *in silico* predictions of Khrenova and colleagues that the double L470T/Q489K and triple V392K/F410V/A426S mutations would lead to a red shift in the excitation and emission spectra of iLOV, we expressed the iLOV$^{L470T/Q489K}$ and iLOV$^{V392K/F410V/A426S}$ mutant proteins in *Escherichia coli* cells and analyzed their fluorescence. We additionally studied the single-point mutant iLOV^{V392K} to assess whether adding a single positive residue in close proximity to the chromophore was sufficient for the red shift. While for the positive controls (GFP and WT iLOV), we could detect fluorescence at the microscope; this was not the case for any of the mutants (Figure 2). We then expressed the same iLOV constructs in mammalian cells, but again no fluorescence was observed except for WT iLOV (Figure S1).

One possibility for the lack of fluorescence could be limited protein expression. Alternatively, the proteins might be well expressed but might be unable to bind the FMN chromophore.

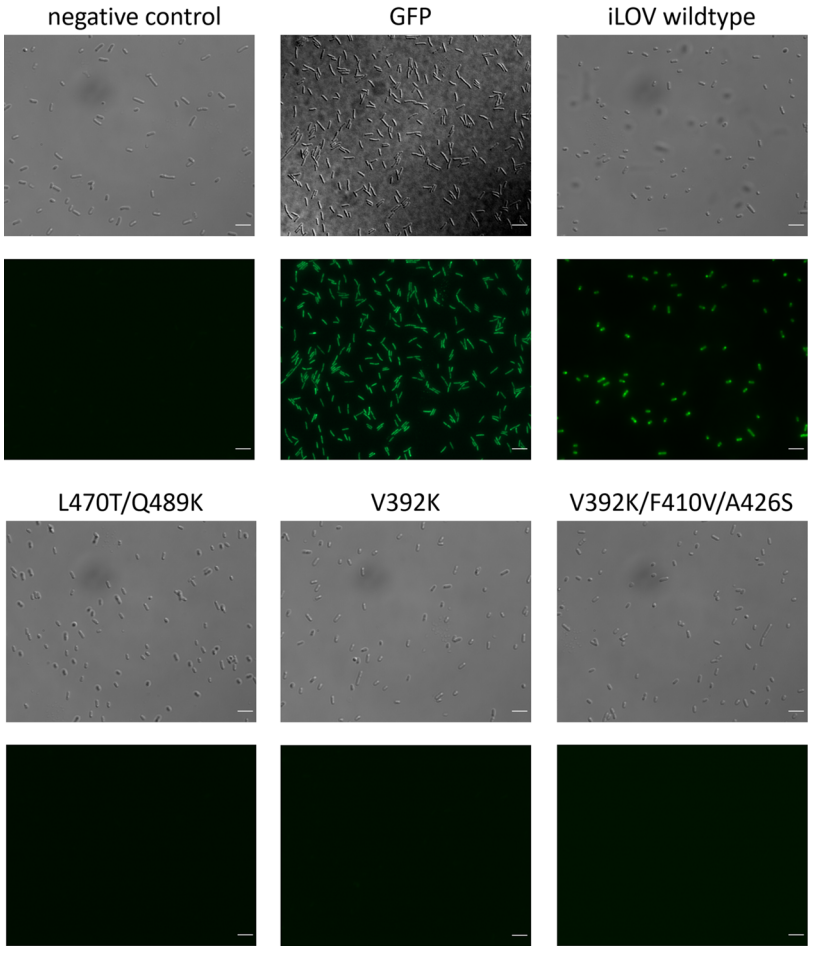

Figure 2. Analysis of the fluorescence of iLOV mutants in *E. coli*. Representative bright-field (top) and GFP channel (bottom) images of *E. coli* Rosetta (DE3) pLysS cells transfected with the indicated constructs. The scale bar for all micrographs is 5 μm. Nontransformed cells were used as the negative control. Cells transformed with a plasmid expressing GFP and WT iLOV, respectively, served as positive controls.

https://doi.org/10.1021/acsomega.2c01283
ACS Omega 2022, 7, 19555−19560

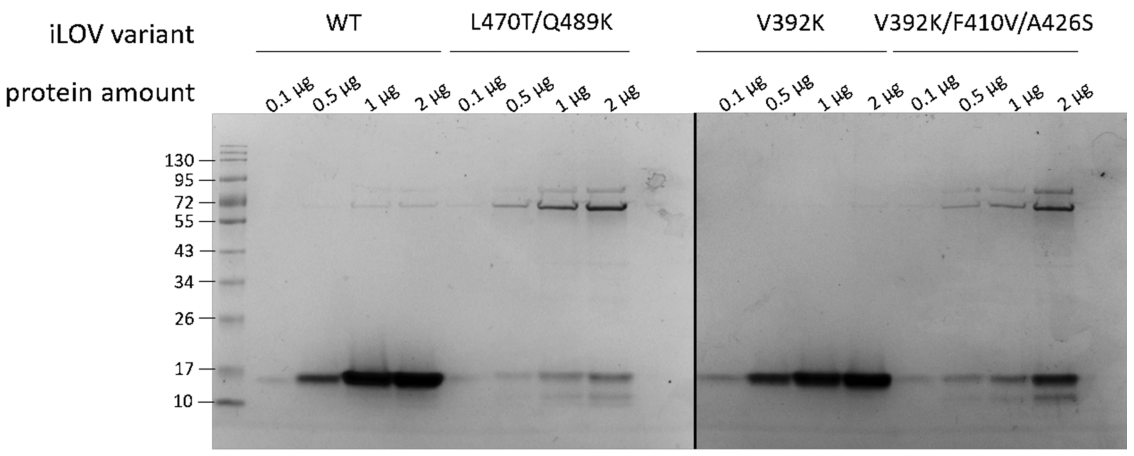

Figure 3. SDS gel of purified proteins. The indicated amounts of proteins were diluted in 10 μL of storage buffer, boiled, and run on a 10% SDS gel. The expected size of all proteins is 15.1 kDa. Pictures of gels were taken with a BIO-RAD ChemiDoc XRS+.

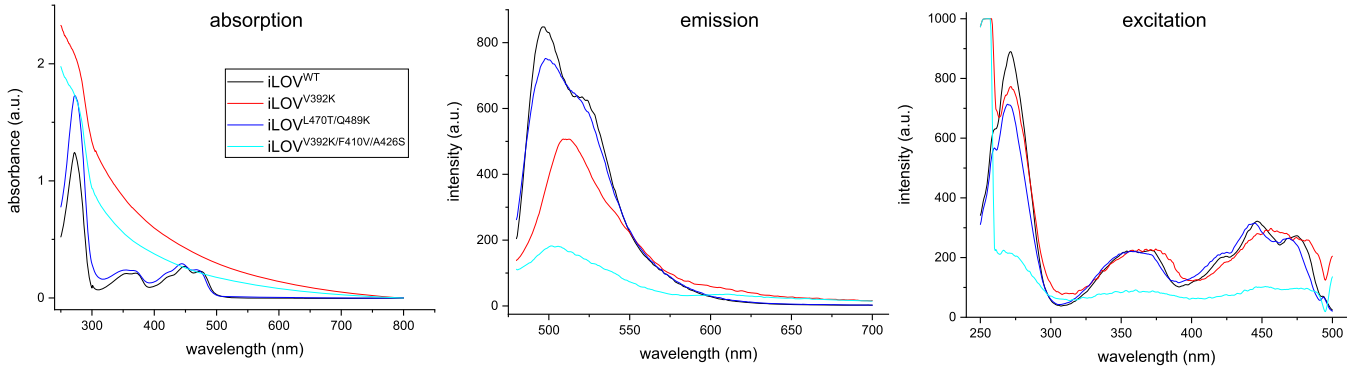

Figure 4. Absorption, excitation, and emission spectra measurements of iLOV mutants. For all purified proteins, absorption spectra were measured between 250 and 800 nm. The excitation and emission spectra measurements were recorded between 250 and 500 nm and 480 and 700 nm, respectively.

Another possibility is that, while FMN can still bind to iLOV, the fluorescence quantum yield is significantly lower. Interestingly, only the pellets of *E. coli* cells overexpressing GFP and WT iLOV appear green to the naked eye (Figure S2). Thus, we aimed to test whether the constructs were expressed at sufficiently high levels, FMN was bound to the proteins, and the fluorescence had sufficient quantum yield.

iLOV$^{L470T/Q489K}$ and iLOV$^{V392K/F410V/A426S}$ Mutants are Expressed at Low Levels Likely Due to Misfolding. To better understand the reasons for the lack of fluorescence, proteins produced from *E. coli* cells were analyzed using an SDS gel (Figure 3). While the WT and the iLOV^{V392K} mutants showed only single bands at around 15 kDa, higher-molecular-weight bands (~70−80 kDa) were observed for the iLOV$^{L470T/Q489K}$ and iLOV$^{V392K/F410V/A426S}$ mutants (Figure 3). Moreover, the iLOV$^{L470T/Q489K}$ mutant had very low concentrations.

To investigate whether the higher-molecular-weight (MW) bands observed in the SDS gels for the double and triple mutants were constituted by the iLOV mutant themselves or other proteins, which co-purified with the mutants, mass spectrometry analysis (MS) of these bands was performed. The results indicated that the high MW bands corresponded to the chaperones GroEL (57.34 kDa) and DnaK (also known as Hsp70; 69.13 kDa) running together with the iLOV mutants (15.1 kDa) leading to a total weight of 72.44 and 84.23 kDa, respectively. GroEL and DnaK have been previously detected in other studies with purified proteins from *E. coli*.[23] Being chaperones, they might be associated with newly synthesized proteins to help them fold properly. Interestingly, visual inspection of the purified proteins showed that only the WT protein fluoresced in a way detectable by the naked eye (Figure S3). To further clarify this observation, optical spectroscopy with the purified proteins was conducted.

Spectroscopic Analyses Indicate that the V392K Mutation Leads to Loss of FMN Binding. Next, we measured the absorption spectrum of all purified iLOV proteins between 250 and 800 nm. Surprisingly, the mutants harboring the V392K mutation, namely, iLOV^{V392K} and iLOV$^{V392K/F410V/A426S}$, did not show the typical FMN peak at 450 nm. Considering that the iLOV^{V392K} mutant was purified as a rather pure protein without contamination according to the SDS gel (Figure 2), these results suggested that mutation to V392K prevents correct folding of the protein and/or its binding to FMN, both essential for fluorescence. This conclusion would be in line with our cell and protein pellet observations indicating no fluorescence in cells with V392K mutation (Figures S2 and S3). In contrast to the QM/MM predictions of Khrenova and colleagues,[20] iLOV$^{V392K/F410V/A426S}$ did not bind FMN, thus showing no fluorescence, and both excitation and emission spectra of iLOV$^{L470T/Q489K}$ were slightly blue-shifted by ~2 nm (Figure 4).

https://doi.org/10.1021/acsomega.2c01283
ACS Omega 2022, 7, 19555−19560

Finally, we determined the quantum yield and the brightness of the WT iLOV and the iLOV$^{L470T/Q489K}$ mutant. The results for WT iLOV were in line with the previous reports.[11] Interestingly, despite the low-expression levels and the co-purification with the chaperone (Figures 2 and 3), iLOV$^{L470T/Q489K}$ exhibited a slightly higher quantum yield and brightness compared to WT iLOV (Table 1).

Table 1. Quantum Yield and Brightness Measurements of WT iLOV and iLOV$^{L470T/Q489K}$[a,b]

	WT	iLOV$^{L470T/Q489K}$
quantum yield (Φ_s)	0.39 ± 0.06 (literature 0.34[11])	0.47 ± 0.07 (0.40 ± 0.07)
brightness	4875 ± 750 (4250)	5875 ± 781 (5000 ± 313)

[a]Numbers in parentheses are calculated by using the literature quantum yield of WT iLOV. [b]Linear regression plots used to calculate quantum yields are given in Figure S4.

DISCUSSION

In this study, we set out to analyze the excitation and emission spectra of two iLOV mutants, iLOV$^{L470T/Q489K}$ and iLOV$^{V392K/F410V/A426S}$, which were computationally predicted to be red-shifted by about 50 nm.[20] We found that the iLOV$^{V392K/F410V/A426S}$ mutant does not bind to FMN and requires chaperones to fold. Our further analysis of iLOV^{V392K} indicates that the V392K mutation causes a loss of FMN binding. Furthermore, the iLOV$^{L470T/Q489K}$ mutant is slightly blue-shifted in both excitation and emission spectra. Initially, Khrenova and colleagues predicted the single mutant iLOV^{Q489K} to be shifted in excitation and emission maxima by 52 and 97 nm, respectively;[18] however, when experimentally measured, the excitation and emission maxima exhibited rather a blue-shift of about 10 nm.[19] This highlighted a disagreement between the predictions and the experimental validations. Even though the QM/MM modeling approach was subsequently updated,[20] our results argue that it is still not able to completely capture the complexity of the interaction between the iLOV$^{L470T/Q489K}$ mutant and its chromophore. Nevertheless, the iLOV$^{L470T/Q489K}$ mutant has an ∼20% increased brightness and quantum yield compared to WT iLOV. These results indicate that L470 and Q489, and probably some other amino acids in the close vicinity, can influence the optical properties of the FMN cofactor in the required direction.

Several studies recently also provided a molecular characterization of the spectral effects of mutations on iLOV to gain a mechanistic understanding.[24−26] Röllen and colleagues have shown that iLOV$^{V392T/Q489K}$ fluorescence has a slight red-shift with an emission spectrum maximum of 502 nm.[26] Similar mutations on iLOV homolog protein CagFbFP$^{I52T/Q148K}$ with the emission maximum of 504 nm and another blue-shifted variant CagFbFP^{Q148K} with the emission maximum of 491 nm were used in fluorescence microscopy experiments and were successfully spectrally separated.[26] While iLOV$^{V392T/Q489K}$ (and its homolog CagFbFP$^{I52T/Q148K}$) was mutated at the same sites as in our study, the V392T mutation may not disrupt FMN binding to iLOV as V392K does. Additionally, while individual mutations such as Q489K may not lead to a red shift alone, they might do so when combined with other mutations.

Previous efforts to improve the properties of iLOV for imaging purposes resulted in the generation of phiLOV, an iLOV derivative with superior photostability, thus solving one of the major drawbacks of WT iLOV.[27] Furthermore, iLOV variants with improved brightness recently have been reported.[14,15] It remains to be seen whether future mutagenesis efforts to red shift iLOV can be combined with these more stable and brighter versions of iLOV.

We believe that the quantification of the fluorescence of large libraries of iLOV mutants would be desirable, as these data (including negative ones, equally informative) could be fed to machine learning algorithms likely to improve the understanding of the residues impacting the spectral properties of iLOV. Previously, similar approaches were successfully applied for improving the brightness of avGFP[28] and YFP.[29]

MATERIAL AND METHODS

Plasmid Construction. Constructs were generated using classical restriction enzyme cloning or golden gate cloning. The *ilov* gene was amplified from iLOV-N1, which was a gift from Michael Davidson (Addgene plasmid #54673; http://n2t.net/addgene:54673; RRID:Addgene_54673), and cloned into pcDNA3.1(+) using *Hin*dIII and *Eco*RI restriction sites, yielding plasmid PL01. PL01 was used as a template to clone all iLOV variants used in this study. Single-point mutations Q489K and V392K were created via overhang PCR yielding PL02 and PL04, respectively. The L470T mutation was introduced into PL02 using golden gate cloning. Amplicons were digested with *Hin*dIII and BpiI, or BpiI and *Eco*RI, respectively, and cloned into pcDNA3.1(+) yielding PL03. The A426S mutation was inserted into PL04 by addition of an *Xba*I restriction site into the coding sequence and cloned into pcDNA3.1(+) yielding PL05. The F410V mutation was introduced using golden gate cloning. Amplicons were digested with *Hin*dIII and BpiI or BpiI and *Eco*RI, respectively, and cloned into pcDNA3.1(+) yielding PL06.

For expression in and purification from *E. coli*, the *ilov*, *ilov*$^{L470T/Q489K}$, *ilov*^{V392K}, and *ilov*$^{V392K/F410V/A426S}$ genes were amplified and then cloned into pET28a using *Nde*I and *Xho*I restriction sites, yielding PL07−PL10. The sequences of all constructs were verified using Sanger sequencing.

Bacterial Cell Culture and Transformation. The bacterial strain used in this study was *E. coli* Rosetta (DE3) pLysS. iLOV constructs were transformed into chemically competent cells via heat shock (42 °C, 1.5 min), plated on lysogeny broth (LB) agar plates containing 0.05 mg/mL kanamycin, and incubated overnight at 37 °C. For expression, 5 mL of liquid LB was inoculated with a single colony from a fresh LB agar plate and incubated overnight at 37 °C and 200 rpm. The next day, the cultures were used to inoculate 1 L of LB with a starting OD600 of 0.1. All liquid media were supplied with 0.05 mg/mL kanamycin.

Protein Expression and Purification. Each pET28a plasmid harboring one iLOV construct was transformed into *E. coli* Rosetta (DE3) pLysS cells and cultures were grown at 37 °C and 220 rpm until they reached an OD600 of 0.4. IPTG (isopropyl-β-D-thiogalactopyranosid) was then added to the culture to a final concentration of 1 mM, and the culture was further grown at 18 °C for 16 h. Afterward, cells were harvested via centrifugation at 5000*g* for 30 min. The pellets were resuspended in a lysis buffer (50 mM KH_2PO_4, pH 7.5, 300 mM NaCl and 10 mM imidazole, pH 8.0) containing one tablet of cOmplete protease inhibitor cocktail (Roche) and lysed by sonication. The lysate was clarified by centrifugation at 20,000*g* for 30 min at 4 °C and loaded onto an IMAC nickel

https://doi.org/10.1021/acsomega.2c01283
ACS Omega 2022, 7, 19555−19560

column (1 mL) using the Bio-Rad NGC automated liquid chromatography system. The column was washed with a wash buffer (same as the lysis buffer but with 20 mM imidazole and 10% glycerol) and eluted with an elution buffer (same as the lysis buffer with further addition of 10% glycerol and 500 mM imidazole). Finally, the elution buffer was replaced with a storage buffer (50 mM HEPES-KOH, pH 7.25, 150 mM KCl, 10% glycerol, 0.1 mM EDTA, pH 8.0) using a P-6 desalting column (10 mL).

Fluorescence Microscopy. Fluorescence microscopy was performed on a Zeiss Axio Observer Z1/7 (Carl Zeiss, Germany) inverted wide-field microscope, equipped with a Colibri 7 LED light source, an α Plan-Apochromat x 100/1.46 oil DIC (UV) M27 objective, filter sets 38 HE (ex. 450−490, dichroic beamsplitter495, em. 500−550; sfGFP), and an Axiocam 506 Mono camera. Six microliters of the culture (OD_{600} = 1.5) was loaded on a glass slide.

SDS Gel and Mass Spectrometry Analyzes of Purified iLOV Proteins. The concentration of purified proteins was determined using NanoDrop One (Thermo Scientific). For performing SDS-PAGE, protein samples were set to contain 0.1, 0.5, 1, and 2 μg, mixed with the Laemmli buffer, and incubated at 95 °C for 15 min. After incubation, the samples were spun down and 20 μL was loaded on a pre-cast 12% agarose gel (MiniProtean TGX gel, BIO-RAD). SDS-PAGE was performed at 130 V for 40 min. Afterward, gels were stained for 1 h using ReadyBlue Protein Gel Stain (Sigma-Aldrich) and destained with ddH_2O overnight. Images were taken with the ChemiDoc XRS+ system (BIO-RAD). Protein bands analyzed using mass spectrometry were excised, treated with 10 mM dithiothreitol and 10 mM iodoacetamide, and subsequently digested with trypsin. The peptide solution was then separated on a Waters Acquity I-class UPLC in positive HD-MSE mode using a Waters Peptide CSH C18 column (2.1 mm × 150 mm, 1.7 μm particle size). A gradient from 1 to 40% ACN/0.1% formic acid (v/v) in water/0.1% formic acid (v/v) was utilized at a starting temperature of 80 °C and a dissolving temperature of 400 °C with a gas flow rate of 800 l/h. Spectra obtained by the separation were analyzed by matching with the UniProt database.

Spectroscopy Analyzes. All optical spectra were measured at room temperature in a fluorescence cuvette with a 1 cm path length (Art. No. 105−250−15−40, Hellma Analytics). Samples (volume 100 μL) with a concentration of 500 μg/mL were dissolved in a storage buffer (50 mM HEPES-KOH, pH 7.25, 150 mM KCl, 10% (v/v) glycerol, 0.1 mM EDTA). Absorption spectra were recorded from 250 to 800 nm (UV-2450 Spectrophotometer, Shimadzu). Fluorescence measurements were performed using a Luminescence Spectrometer (LS 55, Perkin Elmer). Fluorescence excitation spectra were recorded from 250 to 500 nm at a fixed emission wavelength of 496 nm. Emission spectra were measured from 480 to 700 nm at an excitation wavelength of 450 nm. The quantum yields were determined with the comparative method[30,31] using FMN dissolved in the storage buffer as the reference. For the linear regression, the integrated emission (480−700 nm) was plotted against the absorbance at 450 nm. The quantum yield was then calculated using the following equation:

$$\Phi_s = \Phi_r \left(\frac{m_s}{m_r}\right)\left(\frac{\eta_s}{\eta_r}\right)^2$$

where m indicates the slope from the linear regression and η the refractive index of the sample or the reference. The fraction of refractive indices equals 1 since the same buffer was used. For the quantum yield, Φ_r of FMN 0.24 was used.[32] The brightness was calculated as the product of the determined quantum yield and the extinction coefficient of free FMN as 12500 M^{-1} cm^{-1}.[33]

■ ASSOCIATED CONTENT

Supporting Information

The Supporting Information is available free of charge at https://pubs.acs.org/doi/10.1021/acsomega.2c01283.

DNA and amino acid sequences of WT iLOV, $iLOV^{V392K}$, $iLOV^{L470T/Q489K}$, and $iLOV^{V392K/F410V/A426S}$; mammalian cell culture and transient transfection protocols; protocol for the fluorescence microscopy of mammalian cells; analysis of iLOV variants in mammalian cells with fluorescence microscopy (Figure S1); comparison between the pellets of *E. coli* cells expressing different iLOV variants (Figure S2); comparison of the color of iLOV variants (Figure S3); comparative linear regression analysis for quantum yield calculations (Figure S4) (PDF)

■ AUTHOR INFORMATION

Corresponding Author

Mehmet Ali Öztürk − *Institute of Biology II, University of Freiburg, 79104 Freiburg, Germany; Centers for Biological Signalling Studies BIOSS and CIBSS, University of Freiburg, 79104 Freiburg, Germany;* orcid.org/0000-0002-0840-1402; Phone: +49 761 203 2787; Email: mehmet.oeztuerk@bioss.uni-freiburg.de

Authors

Pierre Wehler − *Institute of Biology II, University of Freiburg, 79104 Freiburg, Germany; Centers for Biological Signalling Studies BIOSS and CIBSS, University of Freiburg, 79104 Freiburg, Germany*

Daniel Armbruster − *Institute of Biology II, University of Freiburg, 79104 Freiburg, Germany; Centers for Biological Signalling Studies BIOSS and CIBSS, University of Freiburg, 79104 Freiburg, Germany*

Andreas Günter − *Institute of Physical Chemistry, University of Freiburg, 79104 Freiburg, Germany*

Erik Schleicher − *Institute of Physical Chemistry, University of Freiburg, 79104 Freiburg, Germany*

Barbara Di Ventura − *Institute of Biology II, University of Freiburg, 79104 Freiburg, Germany; Centers for Biological Signalling Studies BIOSS and CIBSS, University of Freiburg, 79104 Freiburg, Germany*

Complete contact information is available at: https://pubs.acs.org/10.1021/acsomega.2c01283

Author Contributions

‖P.W. and D.A. contributed equally to this work.

Funding

This study was funded by the German Ministry for Education and Research (BMBF; grant no. 031L0079 to B.D.V.), by the Excellence Initiative of the German Federal and State Governments BIOSS (EXC-294) and CIBSS (EXC-2189), and by the European Research Council (ERC) under the European Union's Horizon 2020 research and innovation

program (Grant Agreement No. 101002044 to B.D.V.). E.S. would like to thank Hans-Fischer Gesellschaft for continuous support.

Notes

The authors declare no competing financial interest.

■ ACKNOWLEDGMENTS

The authors thank the anonymous reviewers for their constructive feedback during the revision process. They also thank Lena Appel and Matthias Boll (University of Freiburg, Germany) for their mass spectrometry analyses and Alexander Löwer (Max Dellbrück Center for Molecular Medicine, Germany) for sharing the H1299 cell line with them, as well as Michael Davidson (Florida State University, USA) for sharing the iLOV-N1 vector with them.

■ REFERENCES

(1) Shaner, N. C.; Patterson, G. H.; Davidson, M. W. Advances in Fluorescent Protein Technology. *J. Cell Sci.* **2007**, *120*, 4247−4260.
(2) Pédelacq, J.-D.; Cabantous, S.; Tran, T.; Terwilliger, T. C.; Waldo, G. S. Engineering and Characterization of a Superfolder Green Fluorescent Protein. *Nat. Biotechnol.* **2006**, *24*, 79−88.
(3) Shaner, N. C.; Lambert, G. G.; Chammas, A.; Ni, Y.; Cranfill, P. J.; Baird, M. A.; Sell, B. R.; Allen, J. R.; Day, R. N.; Israelsson, M.; Davidson, M. W.; Wang, J. A Bright Monomeric Green Fluorescent Protein Derived from Branchiostoma Lanceolatum. *Nat. Methods* **2013**, *10*, 407−409.
(4) Tsien, R. Y. The Green Fluorescent Protein. *Annu. Rev. Biochem.* **1998**, *67*, 509−544.
(5) Coralli, C.; Cemazar, M.; Kanthou, C.; Tozer, G. M.; Dachs, G. U. Limitations of the Reporter Green Fluorescent Protein under Simulated Tumor Conditions. *Cancer Res.* **2001**, *61*, 4784−4790.
(6) Reid, B. G.; Flynn, G. C. Chromophore Formation in Green Fluorescent Protein. *Biochemistry* **1997**, *36*, 6786−6791.
(7) Chapman, S.; Faulkner, C.; Kaiserli, E.; Garcia-Mata, C.; Savenkov, E. I.; Roberts, A. G.; Oparka, K. J.; Christie, J. M. The Photoreversible Fluorescent Protein ILOV Outperforms GFP as a Reporter of Plant Virus Infection. *Proc. Natl. Acad. Sci. U. S. A.* **2008**, *105*, 20038−20043.
(8) Palanisamy, N.; Öztürk, M. A.; Akmeriç, E. B.; Di Ventura, B. C-Terminal EYFP Fusion Impairs *Escherichia Coli* MinE Function. *Open Biol.* **2020**, *10*, No. 200010.
(9) Roberts, T. M.; Rudolf, F.; Meyer, A.; Pellaux, R.; Whitehead, E.; Panke, S.; Held, M. Identification and Characterisation of a PH-Stable GFP. *Sci. Rep.* **2016**, *6*, No. 28166.
(10) Drepper, T.; Gensch, T.; Pohl, M. Advanced in Vivo Applications of Blue Light Photoreceptors as Alternative Fluorescent Proteins. *Photochem. Photobiol. Sci.* **2013**, *12*, 1125−1134.
(11) Mukherjee, A.; Walker, J.; Weyant, K. B.; Schroeder, C. M. Characterization of Flavin-Based Fluorescent Proteins: An Emerging Class of Fluorescent Reporters. *PLoS One* **2013**, *8*, No. e64753.
(12) Mukherjee, A.; Schroeder, C. M. Flavin-Based Fluorescent Proteins: Emerging Paradigms in Biological Imaging. *Curr. Opin. Biotechnol.* **2015**, *31*, 16−23.
(13) Chia, H. E.; Marsh, E. N. G.; Biteen, J. S. Extending Fluorescence Microscopy into Anaerobic Environments. *Curr. Opin. Chem. Biol.* **2019**, *51*, 98−104.
(14) Ko, S.; Hwang, B.; Na, J.-H.; Lee, J.; Jung, S. T. Engineered Arabidopsis Blue Light Receptor LOV Domain Variants with Improved Quantum Yield, Brightness, and Thermostability. *J. Agric. Food Chem.* **2019**, *67*, 12037−12043.
(15) Ko, S.; Jeon, H.; Yoon, S.; Kyung, M.; Yun, H.; Na, J.-H.; Jung, S. T. Discovery of Novel Pseudomonas Putida Flavin-Binding Fluorescent Protein Variants with Significantly Improved Quantum Yield. *J. Agric. Food Chem.* **2020**, *68*, 5873−5879.
(16) Battad, J. M.; Wilmann, P. G.; Olsen, S.; Byres, E.; Smith, S. C.; Dove, S. G.; Turcic, K. N.; Devenish, R. J.; Rossjohn, J.; Prescott, M. A Structural Basis for the PH-Dependent Increase in Fluorescence Efficiency of Chromoproteins. *J. Mol. Biol.* **2007**, *368*, 998−1010.
(17) Henderson, J. N.; Osborn, M. F.; Koon, N.; Gepshtein, R.; Huppert, D.; Remington, S. J. Excited State Proton Transfer in the Red Fluorescent Protein MKeima. *J. Am. Chem. Soc.* **2009**, *131*, 13212−13213.
(18) Khrenova, M. G.; Nemukhin, A. V.; Domratcheva, T. Theoretical Characterization of the Flavin-Based Fluorescent Protein ILOV and Its Q489K Mutant. *J. Phys. Chem. B* **2015**, *119*, 5176−5183.
(19) Davari, M. D.; Kopka, B.; Wingen, M.; Bocola, M.; Drepper, T.; Jaeger, K.-E.; Schwaneberg, U.; Krauss, U. Photophysics of the LOV-Based Fluorescent Protein Variant ILOV-Q489K Determined by Simulation and Experiment. *J. Phys. Chem. B* **2016**, *120*, 3344−3352.
(20) Khrenova, M. G.; Meteleshko, Y. I.; Nemukhin, A. V. Mutants of the Flavoprotein ILOV as Prospective Red-Shifted Fluorescent Markers. *J. Phys. Chem. B* **2017**, *121*, 10018−10025.
(21) Waterhouse, A.; Bertoni, M.; Bienert, S.; Studer, G.; Tauriello, G.; Gumienny, R.; Heer, F. T.; de Beer, T. A. P.; Rempfer, C.; Bordoli, L.; Lepore, R.; Schwede, T. SWISS-MODEL: Homology Modelling of Protein Structures and Complexes. *Nucleic Acids Res.* **2018**, *46*, W296−W303.
(22) The PyMOL Molecular Graphics System *PyMOL*, version 1.7.2.1; Schrödinger, LLC, 2014.
(23) Calloni, G.; Chen, T.; Schermann, S. M.; Chang, H.-C.; Genevaux, P.; Agostini, F.; Tartaglia, G. G.; Hayer-Hartl, M.; Hartl, F. U. DnaK Functions as a Central Hub in the *E. coli* Chaperone Network. *Cell Rep.* **2012**, *1*, 251−264.
(24) Goncharov, I. M.; Smolentseva, A.; Semenov, O.; Natarov, I.; Nazarenko, V. V.; Yudenko, A.; Remeeva, A.; Gushchin, I. High-Resolution Structure of a Naturally Red-Shifted LOV Domain. *Biochem. Biophys. Res. Commun.* **2021**, *567*, 143−147.
(25) Remeeva, A.; Nazarenko, V. V.; Kovalev, K.; Goncharov, I. M.; Yudenko, A.; Astashkin, R.; Gordeliy, V.; Gushchin, I. Insights into the Mechanisms of Light-Oxygen-Voltage Domain Color Tuning from a Set of High-Resolution X-Ray Structures. *Proteins* **2021**, *89*, 1005−1016.
(26) Röllen, K.; Granzin, J.; Remeeva, A.; Davari, M. D.; Gensch, T.; Nazarenko, V. V.; Kovalev, K.; Bogorodskiy, A.; Borshchevskiy, V.; Hemmer, S.; Schwaneberg, U.; Gordeliy, V.; Jaeger, K.-E.; Batra-Safferling, R.; Gushchin, I.; Krauss, U. The Molecular Basis of Spectral Tuning in Blue- and Red-Shifted Flavin-Binding Fluorescent Proteins. *J. Biol. Chem.* **2021**, *296*, No. 100662.
(27) Christie, J. M.; Hitomi, K.; Arvai, A. S.; Hartfield, K. A.; Mettlen, M.; Pratt, A. J.; Tainer, J. A.; Getzoff, E. D. Structural Tuning of the Fluorescent Protein ILOV for Improved Photostability. *J. Biol. Chem.* **2012**, *287*, 22295−22304.
(28) Biswas, S.; Khimulya, G.; Alley, E. C.; Esvelt, K. M.; Church, G. M. Low-N Protein Engineering with Data-Efficient Deep Learning. *Nat. Methods* **2021**, *18*, 389−396.
(29) Saito, Y.; Oikawa, M.; Nakazawa, H.; Niide, T.; Kameda, T.; Tsuda, K.; Umetsu, M. Machine-Learning-Guided Mutagenesis for Directed Evolution of Fluorescent Proteins. *ACS Synth. Biol.* **2018**, *7*, 2014−2022.
(30) Williams, A. T. R.; Winfield, S. A.; Miller, J. N. Relative Fluorescence Quantum Yields Using a Computer-Controlled Luminescence Spectrometer. *Analyst* **1983**, *108*, 1067−1071.
(31) Homans, R. J.; Khan, R. U.; Andrews, M. B.; Kjeldsen, A. E.; Natrajan, L. S.; Marsden, S.; McKenzie, E. A.; Christie, J. M.; Jones, A. R. Two Photon Spectroscopy and Microscopy of the Fluorescent Flavoprotein, ILOV. *Phys. Chem. Chem. Phys.* **2018**, *20*, 16949−16955.
(32) Kotaki, A.; Yagi, K. Fluorescence Properties of Flavins in Various Solvents. *J. Biochem.* **1970**, *68*, 509−516.
(33) Drepper, T.; Eggert, T.; Circolone, F.; Heck, A.; Krauss, U.; Guterl, J.-K.; Wendorff, M.; Losi, A.; Gärtner, W.; Jaeger, K.-E. Reporter Proteins for in Vivo Fluorescence without Oxygen. *Nat. Biotechnol.* **2007**, *25*, 443−445.

https://doi.org/10.1021/acsomega.2c01283
ACS Omega 2022, 7, 19555−19560